Reflection-free propagation of wave packets

S. Yoshida,[1,2] S. Watanabe,[1,3] C. O. Reinhold,[1,2] and J. Burgdörfer[1,2,4]
[1]*Department of Physics, University of Tennessee, Knoxville, Tennessee 37996-1200*
[2]*Physics Division, Oak Ridge National Laboratory, Oak Ridge, Tennessee 37831-6373*
[3]*Department of Applied Physics, University of Electro-communications, 1-5-1 Chofugaoka, Chofu-shi, Tokyo 182-8585, Japan*
[4]*Institute for Theoretical Physics, Vienna University of Technology, A1040 Vienna, Austria*
(Received 10 November 1998)

We analyze the problem of suppression of reflections within the numerical propagation of wave packets using finite atomiclike pseudostate expansions. Artificial reflections at effective ''walls'' and reentering of probability flux into the interaction region represents a major limitation for the study of long-time evolution of atomic ionization processes. We propose two methods, the repetitive projection method (RPM) and Siegert pseudostate (SPS) propagation, and study their efficiency in suppressing reflections. It is shown that the quantum Zeno effect sets a limit on the efficiency of the RPM as well as of masking functions. For the exactly solvable propagation of a radial-free wave packet, we show that both the SPS and the RPM provide almost complete suppression of reflections without appreciable distortion in the physically relevant region of coordinate space. [S1050-2947(99)03908-6]

PACS number(s): 32.80.Fb, 31.15.−p, 32.80.Rm, 02.70.−c

I. INTRODUCTION

For a large number of dynamical atomic processes, the numerical solution of the time-dependent Schrödinger equation requires the propagation of ''free'' wave packets out to large times and large distances. Only at that point does projection onto asymptotic final states allow the unambiguous determination of transition amplitudes and, hence, of the *T* or *S* matrix. These include ionization of atoms by charged particles, photons, and intense electromagnetic fields. In all cases, the nonstationary wave packet contains a continuum component which will eventually escape the interaction region. Numerical representations of the wave packet in terms of a finite basis set, either in terms of atomic pseudostates or lattice-based representations, have the fundamental limitation that they subtend only a finite domain in coordinate space up to a certain distance *R*. Therefore, any finite basis representation contains a ''wall'' or boundary at *R*, either explicitly in box or lattice representations or implicitly in pseudostate representations, at which the continuum portion of the wave packet will eventually be reflected and will reenter the interaction region, thereby artificially distorting the bound-state portion of the evolved wave packet. Depending on the method used, the wall may be hard or soft and its efficient position may depend on the momentum and energy of the wave packet. While this problem is ubiquitously present in all numerical propagation schemes, it is of relatively little influence in the study of transitions into low-energy states and short times. It becomes, however, a major hurdle for long interaction times and problems involving highly excited states such as Rydberg states.

Suppression of reflections is particularly important in investigations of the classical-quantum correspondence of Hamiltonian systems with mixed phase space. The ''discordance'' between the quantum evolution with the corresponding classical system exhibiting ''soft chaos'' should manifest itself for sufficiently long times of the order of the so-called Heisenberg times $t_H \approx \hbar/\langle \Delta E \rangle$ where $\langle \Delta E \rangle$ is the typical mean level spacing of a system [1]. In order to delineate the breakdown of classical-quantum correspondence, the challenge is to integrate the time-dependent Schrödinger equation (TDSE) out to times longer than t_H. This time typically exceeds the time when the first reflections in the basis set have occurred. One prototype system where we encountered the difficulty is the periodically kicked atom, a paradigm of quantum chaos in atomic physics [2–6]. It is therefore crucial to control and suppress reflections at the walls without distortion of the wave packet evolution in the physically relevant region of coordinate space where the classical-quantum correspondence is being investigated.

In this paper we report new alternative techniques for the suppression of boundary reflections in the quantum evolution within the framework of atomic pseudostate representations, namely, the repetitive projection method (RPM) and the Siegert pseudostate (SPS) propagation. Unlike for lattice-based methods, controlling reflections within pseudostate expansions is less straightforward and poorly understood since the boundary is only implicitly determined. We study their efficiency in suppressing reflections and we discuss their connection with standard methods such as masking functions and optical potentials as well as complex rotation [7–18]. It is shown that the quantum Zeno effect sets a limit on the efficiency of the RPM as well as of masking functions. We show that both RPM and SPS can (almost) completely suppress reflections without appreciably perturbing the ''inner'' region. As a test case, we use the time propagation of a free particle which can be calculated analytically and which captures the essence of the problem. Atomic units are used throughout.

II. COUPLED-STATE METHOD FOR THE SOLUTION OF THE TDSE

Consider the dynamics of a particle with coordinate $\vec{r}$ and Hamiltonian *H*. One of the most versatile and most frequently employed techniques to numerically solve a time-

 ©1999 The American Physical Society

dependent Schrödinger equation is the coupled-state method. Its core ingredient is a finite basis expansion of the wave function as

$$|\psi(t)\rangle = \sum_{n=1}^{N} a_n(t)|\phi_n\rangle, \tag{1}$$

where N is the number of basis states $|\phi_n\rangle$ included in the truncated expression. Equation (1) converts the TDSE into a system of coupled ordinary differential equations of the form

$$i\dot{\vec{a}}(t) = \hat{H}\vec{a}(t), \tag{2}$$

where $\vec{a}(t)=(a_1,\ldots,a_n,\ldots,a_N)$ is the state vector, and $\hat{H}(t)$ is the Hamiltonian matrix with elements $\langle\phi_n|H|\phi_{n'}\rangle$. In Eq. (2) and in the following we assume that the basis set is orthonormal [if the basis functions are nonorthogonal, Eq. (2) also contains the overlap matrix with elements $\langle\phi_n|\phi_{n'}\rangle$].

The key point for the following analysis is that in any truncated expansion of the form (1) where N is finite (limited by present computational capabilities) only a finite domain in coordinate space up to a radius $r \lesssim R$ can be adequately represented. Thus, as the wave function expands in time, it becomes reflected as it reaches this boundary. Here we study a few techniques, old and new, for avoiding these reflections using various square integrable basis functions $|\phi_n\rangle$. For simplicity, we apply these methods to the evolution of a free particle and we assume that N refers to the number of basis states in the radial direction, thereby ignoring the basis states required to subtend the angular degrees of freedom. For zero angular momentum, the problem is equivalent to that of a free one-dimensional (1D) particle with Hamiltonian

$$H = -\frac{1}{2}\frac{d^2}{dr^2}, \tag{3}$$

and the boundary condition on the wave function $\psi(0,t)=0$ for all t. It should be kept in mind, however, that in realistic 3D calculations a total number of N basis states have to be distributed among all degrees of freedom such that only $\sim N^{1/3}$ states are available in the radial direction. In other words, just increasing N is not a viable option to control the problem of reflections.

It is useful to distinguish two different classes of basis states.

(a) Strongly localized basis expansions greatly simplify the evaluation coordinate operators such as arbitrary potentials or masking functions. They include, among others, lattice expansions [9,10] and discrete variable representations (DVR) [19]. In each case, $\phi_n^G(r)$ is effectively localized at one grid point r_n of the lattice and the matrix representation of an operator $O(r)$ is diagonal,

$$\langle\phi_m^G|O(r)|\phi_n^G\rangle \propto \delta_{m,n}O(r_n). \tag{4}$$

(b) Pseudostate expansions, on the other hand, are delocalized within a finite domain of coordinate space with a variable number of nodes, typically $\phi_n(r)$ contains $n-1$ radial nodes. A prototype is the set of radial box (B) wave functions for a box of radius R,

$$\langle r|\phi_n^B\rangle = \phi_n^B(r) = \sqrt{\frac{2}{R}}\sin(p_n r), \tag{5}$$

with $p_n=\pi n/R$. Another example of atomic pseudostates which we discuss in the following is the Sturmian (S) pseudostates [15,16,20]

$$\langle r|\phi_n^S\rangle = \phi_n^S(r) = \frac{2}{n\sqrt{n_S}}\frac{r}{n_S}e^{-r/n_S}L_{n-1}^1(2r/n_S), \tag{6}$$

where n_S is referred to as the Sturmian parameter. The specific advantage of the Sturmian expansion is that for properly chosen n_S, a single ϕ^S can represent a hydrogenic atomic state for a given quantum number with its nodal structure (for $n_S=n$ the equivalence is exact) and it properly describes a Coulomb singularity for $r\to 0$. Moreover, for any fixed n_S the discrete set is complete and its truncation at N yields a discrete representation of a portion of the continuum [15,16,20,21].

One common feature of all these expansions is the presence of a ''wall'' at some value $r\simeq R$. For lattice-based expansions, reflections occur at or near the outermost grid point, i.e., $r_N=R$. For box wave functions, R is obviously given by the wall of the box, while for atomic pseudostates of Sturmian type the wall is ''soft'' and its location is less obvious. It can be estimated from the radial expectation values for Sturmian pseudostates

$$\langle r\rangle_n = \langle\phi_n^S|r|\phi_n^S\rangle = \frac{3}{2}nn_S \leqslant \frac{3}{2}Nn_S. \tag{7}$$

The position of the wall is therefore of the order of $\langle r\rangle_N$ and scales linearly with n_S. In fact, the effective position of the wall is energy (or momentum) dependent since the local density of states (LDOS) varies with the distance from the origin. For a simple estimate we use the asymptotic expression of $\phi_n^S(r)$ for large r and n [22],

$$\lim_{r,n\to\infty}\phi_n^S(r) \propto \cos(\sqrt{8nr/n_S}-3\pi/4). \tag{8}$$

Near $r=n_S n$ the local wavelength is approximately given by

$$\lambda \simeq \sqrt{2}\pi n_S \tag{9}$$

corresponding to an n-independent local momentum

$$\langle p\rangle \approx \sqrt{2}/n_S. \tag{10}$$

Combining Eq. (10) with Eq. (7) leads to the relation

$$\langle p\rangle \ \langle r\rangle_n \lesssim 2N \tag{11}$$

for the momentum dependence of the effective position of the ''reflecting wall.'' A more detailed quantitative analysis of this problem will be given below. The physical significance of Eq. (11) is that reflections set in when the characteristic wavelength of the wave packet can no longer be accommodated even when the spatial extent of the truncated basis reaches farther out. The fact that for atomic pseudostates the effective position of the wall is a dynamic rather than just a purely geometric quantity may be one of the

reasons why systematic investigations of the problem of reflections in atomic pseudostate expansions appear to be missing.

III. SUPPRESSING REFLECTIONS

Suppose that the full Hilbert space of square integrable functions is divided into P and Q subspaces such that $\{P\}=\{\phi_n;n=1,\ldots,N\}$ is the subspace subtended by our finite basis set and

$$1=|P+Q\rangle\langle P+Q|=|P\rangle\langle P|+|Q\rangle\langle Q|, \tag{12}$$

$$|P\rangle\langle P|=\sum_{n=1}^{N}|\phi_n\rangle\langle\phi_n|. \tag{13}$$

The task is to find a good approximation for the projection of the wave function onto the subspace P which is given by

$$|\psi(t)\rangle_P=|P\rangle\langle P|\psi(t)\rangle=|P\rangle\langle P|e^{-iHt}|P\rangle\langle P|\psi(0)\rangle, \tag{14}$$

where we have assumed that the initial state $|\psi(0)\rangle$ of the wave packet is well localized in our basis set, i.e.,

$$|\psi(0)\rangle\simeq|P\rangle\langle P|\psi(0)\rangle, \tag{15}$$

$$\langle Q|\psi(0)\rangle\simeq 0. \tag{16}$$

Note that apart from this assumption, the wave function $|\psi(t)\rangle_P$ is exact. It differs from the coupled-state solution of Eq. (2) which is given by $\vec{a}(t)=\exp(-i\hat{H}t)\vec{a}(0)$ or, in the present notation, $\vec{a}(t)=\langle P|\psi(t)\rangle$, $\hat{H}=\langle P|H|P\rangle$,

$$|\psi^U(t)\rangle_P=|P\rangle e^{-i\langle P|H|P\rangle t}\langle P|\psi(0)\rangle, \tag{17}$$

due to the different evolution operators

$$\exp(-i\langle P|H|P\rangle t)\neq\langle P|\exp(-iHt)|P\rangle. \tag{18}$$

The matrix representation of the evolution operator within the P space [left-hand side of inequality (18)] is unitary and does not allow for any flux of probability outside the P space. In turn, the right hand side, $\langle P|\exp(-iHt)|P\rangle$, is not unitary since it is a representation of the exact evolution operator which allows for coupling to the Q space. The differences between Eqs. (17) and (14) can be made more explicit by expressing the wave function in terms of the eigenvectors of the evolution operators:

$$|\psi(t)\rangle_P=\sum_{k=1}^{N}b_k(0)e^{-iE_kt}|\chi_k\rangle, \tag{19}$$

$$|\psi^U(t)\rangle_P=\sum_{k=1}^{N}c_k(0)e^{-i\epsilon_kt}|\varphi_k\rangle. \tag{20}$$

In Eq. (20), ϵ_k denotes the real eigenvalue of the Hamiltonian $\langle P|H|P\rangle$. In Eq. (19), on the other hand, E_k is defined through the relation

$$\langle P|\exp(-iHt)|P\rangle\langle P|\chi_k\rangle=\exp(-iE_kt)\langle P|\chi_k\rangle. \tag{21}$$

The nonunitarity is reflected in the complex eigenvalues $E_k=E_k=E_k^R+iE_k^I$. Suppression of reflection in the exact evolution operator can therefore be attributed to the presence of an imaginary part of the effective spectrum that eliminates probability from the P space. The basic ingredient to all approximate prescriptions for controlling reflection is the introduction of a nonunitary operator whose effect is to eliminate probability flux that is associated with the reflecting portion of the wave packet. Within a coupled-state approach, for example, a non-Hermitian interaction can be added to the Hamiltonian to induce the nonunitary evolution. Such additional terms are often referred to as ''relaxation operators'' or ''optical potentials.'' For a faithful representation of the long-time evolution, it is essential that the effect of the relaxation operator be confined to the region of the wall and not disturb the evolution in the ''inner'' region.

A. Masking functions

For lattice-based localized basis expansions [Eq. (4)], the choice of relaxation operators is straightforward. We briefly discuss their properties before turning to the construction of the corresponding operators for atomic pseudostate expansions, which is the main focus of this investigation. At the most elementary level, a relaxation operator can be constructed by a masking function [7–10]. Let $\mathcal{M}(r)$ be a masking function so that

$$\mathcal{M}(r)=\begin{cases}1 \text{ if } r<r_N\\ f(r)<1 \text{ if } r_{N+1}\leqslant r\leqslant r_M.\end{cases} \tag{22}$$

The range of lattice sites $r_{N+1},\ldots,r_M$ close to the reflecting wall now represent a finite Q' subspace ($Q'\subset Q$) that corresponds to a finite number of lattice sites beyond the P subspace ($r<r_N$). In Q' the wave function is allowed to relax by way of an amplitude-absorbing mask. The masking function $f(r)$ can be chosen to be continuously differentiable at r_N to high order in order to minimize effects of discontinuities. Masking is effected by simply multiplying the state vector after every time interval Δt_j by the masking operator $\mathcal{M}$ which is diagonal in the lattice basis ϕ_k:

$$|\psi^{\mathcal{M}}(t)\rangle_P=|P\rangle\langle P|P+Q'\rangle\left(\prod_{j=1}^{J}\mathcal{M}\,e^{-i\langle P+Q'|H|P+Q'\rangle\Delta t_j}\right)\times\langle P+Q'|\psi(0)\rangle, \tag{23}$$

with

$$t=\sum_{j=1}^{J}\Delta t_j\ . \tag{24}$$

The application of $\mathcal{M}$ is equivalent to a nonunitary evolution operator

$$U^{\mathcal{M}}=\exp(\ln\mathcal{M})=\exp(-iV_{\text{opt}}\Delta t) \tag{25}$$

generated by an optical potential V_{opt}

$$V_{\text{opt}}=i(\ln\mathcal{M})/\Delta t\ . \tag{26}$$

We note that masking functions introduce a specific class of optical potentials which can be expressed in terms of Eq. (26). However, an arbitrary smooth optical potential cannot, in general, be reduced to a simple masking function [Eq. (22)]. $U^{\mathcal{M}}$ does not explicitly depend on Δt [Eq. (25)]. Implicitly, however, Δt enters through the application of the masking operator after every time interval Δt. From Eqs. (22) and (26) it is obvious that the spectrum of $V_{\rm opt}$ lies on the negative imaginary axis. For $\Delta t \to 0$, $V_{\rm opt}$ seemingly becomes infinitely absorptive [Eq. (26)]. However, we will discuss below how Eqs. (25) and (26) imply complete reflection in the limit $\Delta t \to 0$. This result, somewhat surprising at first glance, is connected to the quantum Zeno effect.

B. Repetitive projection method

The implementation of the analog to masking into atomic pseudostate expansions is not obvious because of the delocalized nature of the basis states. No particular subset of the basis can be directly associated with spatial region near the boundary. Consequently, the relaxation operator will be, in general, nonlocal and nondiagonal with respect to the basis. The construction of such a relaxation operator is clearly not unique. We show in the following that repetitive projection onto a conveniently chosen subspace provides a realization of a relaxation operator or, equivalently, of an optical potential. We implement this method for the Sturmian basis set [Eq. (6)]. Many features of this repetitive projection method are, however, valid for other basis sets as well.

The starting point is the observation that radial expectation values are ordered with quantum numbers [Eq. (7)]. Consequently, despite the delocalized nature and nodal structure of the basis states, one can associate the Sturmian states with the largest quantum numbers with the probability amplitude in the region of coordinate space closest to the effective wall. We therefore decompose the truncated Hilbert space into two finite subspaces

$$\{P\}=\{\phi_n^S\}_{i\leq n\leq N},\qquad \{Q'\}=\{\phi_n^S\}_{N+1\leq n\leq M}, \tag{27}$$

with the description of the unity within the M-dimensional model space [i.e., Eq. (12) but for a finite Q' space]. The P space represents the interaction region or inner region where the initial state $|\psi(0)\rangle$ of the wave packet is localized [i.e., Eq. (15)].

After a time step Δt, we project the time evolution in the model space $P+Q'$ onto P,

$$|\psi^{\rm RPM}(\Delta t)\rangle_P=|P\rangle\langle P|P+Q'\rangle e^{-i\langle P+Q'|H|P+Q'\rangle\Delta t}\times\langle P+Q'|P\rangle\langle P|\psi(0)\rangle. \tag{28}$$

That is, from the evolved wave packet we now remove the component that has reached the Q' space, the boundary region, much like for the exact wave function (14) for which the $P+Q'$ space would be the full Hilbert space of square integrable functions. Repeating this process for a total of J time intervals Δt_j (not necessarily equal) leads to

$$|\psi^{\rm RPM}(t)\rangle_P=|P\rangle\left(\prod_{j=1}^{J}\langle P|P+Q'\rangle e^{-i\langle P+Q'|H|P+Q'\rangle\Delta t_j}\times\langle P+Q'|P\rangle\right)\langle P|\psi(0)\rangle. \tag{29}$$

Note that the domain of the Hamiltonian is the full model space $P+Q'$. Moreover, H is not block-diagonal with respect to the $P-Q'$ decomposition, i.e.,

$$H=|P\rangle\langle P|H|P\rangle\langle P|+|Q'\rangle\langle Q'|H|P\rangle\langle P|+|P\rangle\langle P|H|Q'\rangle\times\langle Q'|+|Q'\rangle\langle Q'|H|Q'\rangle\langle Q'|, \tag{30}$$

where $\langle P|H|Q'\rangle=\langle Q'|H|P\rangle^*$ because of Hermiticity. Within each time interval, the Hamiltonian couples the wave packet to the full $P+Q'$ space including the ''boundary region'' represented by the Q' space. After each projection, only the portion of the wave function remaining in the inner region is kept. Equation (29) is the central result for the RPM.

It is easy to show that this method is formally equivalent to masking. The projection operator can be associated with a nonunitary masking operator

$$\mathcal{M}=|P\rangle\langle P|. \tag{31}$$

The corresponding optical potential follows from

$$e^{-iV_{\rm opt}\Delta t}=|P\rangle\langle P| \tag{32}$$

as

$$V_{\rm opt}=\frac{i}{\Delta t}\ln(|P\rangle\langle P|). \tag{33}$$

Since the spectrum of the projection operator is positive definite and bounded from above by 1, the spectrum of $V_{\rm opt}$ lies again on the negative imaginary axis. However, unlike masking functions in coordinate space, this optical potential introduces also masking in momentum (or energy) space.

C. Complex rotation method

As has been pointed out some time ago [12], complex coordinate scaling provides a method to suppress reflections. Complex scaling involves the following canonical transformation in the complex plane [13,14]: The position r and momentum p are rotated by an angle θ into the complex plane,

$$r\to re^{i\theta}, \tag{34}$$

and

$$p\to pe^{-i\theta}. \tag{35}$$

Correspondingly, the basis functions are rotated as

$$\phi_n(r)\to\phi_n^\theta(r)=\phi_n(re^{i\theta}), \tag{36}$$

which are usually referred to as complex basis functions [12–14]. For Sturmian pseudostates, the complex rotation (CR) of r is equivalent to using a complex Sturmian param-

eter $n_S^\theta = n_S \exp(-i\theta)$ [15]. It can be shown that the projection of the wave function onto the P space is equivalent to

$$|\psi(t)\rangle_P = e^{-iHt}|\psi(0)\rangle = |P(-\theta)\rangle\langle P(-\theta)|e^{-iHt}|P(-\theta)\rangle \times\langle P(-\theta)|\psi(0)\rangle, \tag{37}$$

where the subspace $\{P(\theta)\}$ corresponds to the set $\{\phi_n^\theta\}$. Using the property

$$\langle \phi_n^{-\theta}|H|\phi_m^{-\theta}\rangle = \int d(re^{-i\theta})\phi_n(re^{-i\theta})H\phi_m(re^{-i\theta}) = \int dr\,\phi_n(r)H(\theta)\phi_m(r) = \langle \phi_n|H(\theta)|\phi_m\rangle, \tag{38}$$

and the approximation $\langle P(-\theta)|\exp(-iHt)|P(-\theta)\rangle \simeq \exp[-i\langle P(-\theta)|H|P(-\theta)\rangle t]$, one finally arrives at

$$|\psi^{\mathrm{CR}}(t)\rangle_P \simeq |P(-\theta)\rangle e^{-i\langle P|H(\theta)|P\rangle t}\langle P(-\theta)|\psi(0)\rangle \tag{39}$$

or, equivalently,

$$\psi^{\mathrm{CR}}(r,t) = \sum_{n=1}^{N} c_n^\theta(0) e^{-iE_n t}\varphi_n(re^{-i\theta}), \tag{40}$$

where the initial state is supposed to be contained in the rotated basis and φ_n are the eigenvectors of the Hamiltonian [Eq. (20)]. These equations are seemingly very similar to Eqs. (17) and (20). However, the rotated Hamiltonian $H(\theta)$ is no longer Hermitian. Upon rotation of p,

$$H = -\frac{1}{2}\frac{d^2}{dr^2} \rightarrow H(\theta) = -\frac{1}{2}e^{-2i\theta}\frac{d^2}{dr^2}\ , \tag{41}$$

the solutions $|\varphi_n\rangle$ of the energy eigenvalue equation now yield complex eigenvalues. The free-particle continuum is rotated into the lower half plane,

$$k \rightarrow k = k_R + ik_I = |k|(\cos\theta - \imath\sin\theta), \tag{42}$$

$$E = \frac{k^2}{2} \rightarrow \frac{|k|^2}{2}e^{-2i\theta} = E^R + i\,E^I, \tag{43}$$

with

$$E^R = \frac{1}{2}(k_R^2 - k_I^2) = \frac{1}{2}|k|^2\cos 2\theta, \tag{44}$$

$$E^I = k_R k_I = -\frac{1}{2}|k|^2\sin 2\theta. \tag{45}$$

All positive-energy discrete eigenvalues of the Hamiltonian in the pseudostate basis lie on a ray emanating from the origin and making an angle of -2θ with the positive (real) energy axis (Fig. 1). The free-particle continuum states are square integrable and satisfy, apart from exponential damping at large distances, outgoing boundary conditions $\sim e^{irk_R}e^{-r|k_I|}$. This property suggests that complex rotation may also be well suited for describing the reflection-free propagation of the wave packet.

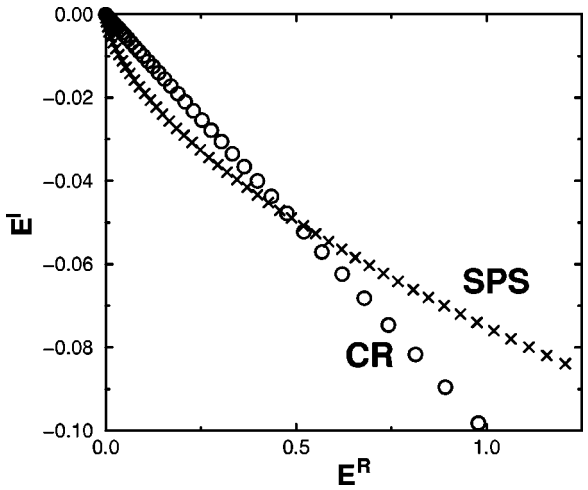

FIG. 1. The energy spectrum of the free-particle Hamiltonian calculated with an $N=50$ Siegert pseudostate expansion (crosses) and the complex rotation method using $N=70$ Sturmian functions (circles). The rotation angle for the complex rotation method is $\theta = 0.05$ rad and the Sturmian parameter is $n_S = 1$.

D. Siegert pseudostate expansions

The Siegert states have played an important role in the theory of scattering for a long time. For instance, Schneider [23] proposed the calculation of resonances in time-independent scattering theory employing Siegert pseudostates. More recently, generating Siegert pseudostates as eigenvectors of a generalized eigenvalue problem has been proposed by Tolstikhin *et al.* [24], and a fuller account of its mathematical structure and results have been given in [25]. Siegert pseudostates are, in fact, closely related to the box states [Eq. (5)] where the standing-wave boundary condition at R is replaced by purely outgoing-wave boundary conditions. The radial Schrödinger equation within the interval $[0,R]$ which defines Siegert states

$$\left[-\frac{1}{2}\frac{d^2}{dr^2} + V(r) - E\right]\phi(r) = 0, \quad E = \frac{1}{2}k^2 \tag{46}$$

is solved subject to the boundary conditions

$$\phi(r)|_{r=0} = 0, \qquad \left(\frac{d}{dr} - ik\right)\phi(r)|_{r=R} = 0. \tag{47}$$

In the present case of the free radial wave packet evolution, we choose

$$V(r) = \begin{cases} 0, & r < R \\ v_0 > 0, & r = R \end{cases} \tag{48}$$

where v_0 is small but finite. We show that SPSs are particularly well suited to control reflections. The obvious advantage of a truncated set of SPSs is that the outgoing boundary conditions explicitly suppress reflections. The price to be paid is that the square root of the eigenenergy (i.e., k) appears in the boundary condition. This leads to a quadratic eigenvalue problem where k is now, in general, complex.

The solution of the Siegert pseudostate eigenvalue problem proceeds by expansion into DVR basis functions $\pi_i(r)$,

$$\phi_n(r)=\sum_i \beta_{n,i}\sqrt{w(r)}\pi_i(r), \tag{49}$$

where $\pi_i(r)$ is a strongly localized function on the grid satisfying

$$\pi_i(r_j)=0,\ i\neq j \tag{50}$$

and $w(r)$ is a weighting function in the orthogonality relation of polynomials from which the DVR functions are constructed. Details can be found in Ref. [25]. Our Siegert basis set is constructed from the eigenvalues of Eq. (46) using the N smallest values for the absolute magnitude of the eigenenergies. Note that in order to accurately calculate these N Siegert states, one needs to perform a calculation using a larger DVR basis set. Usually one uses $\tilde{N}$ DVR states from which one keeps only N Siegert eigenstates with the lowest eigenenergies, discarding the rest. In the following, we use $\tilde{N}=100$ DVR basis functions and retain $N=50$ Siegert states.

Within the SPS approach, the projection of the wave function in the P subspace (i.e., the $[0,R]$ subspace) can be expressed as

$$\psi^{\mathrm{SPS}}(r,t)=\sum_{n=1}^{N} c_n(0)e^{-iE_nt}\phi_n(r), \tag{51}$$

where the eigenenergies E_n are complex numbers. We give in Fig. 1 the complex energy spectrum for the SPS states. For a free particle in a box with a small, but finite, value v_0 of the potential at the boundary [Eqs. (46)–(48)], the eigenvalue equation can be expressed as

$$\xi=n\pi-\frac{i}{2}\ln\frac{\sqrt{\xi^2-\epsilon^2}+\xi}{\sqrt{\xi^2-\epsilon^2}-\xi}, \tag{52}$$

where

$$\begin{aligned}\xi&=kR,\\ \epsilon^2&=2v_0R^2.\end{aligned} \tag{53}$$

Solving this by iteration, the first iteration yields

$$k=\frac{\xi}{R}\simeq\frac{1}{R}\left[\left(n+\frac{1}{2}\right)\pi-i\ln\frac{\sqrt{2}n\pi}{\sqrt{v_0}R}\right], \tag{54}$$

where $\epsilon\ll|\xi|$. The iteration may be continued until a desired degree of convergence is achieved. As indicated by the first-order iteration formula [Eq. (54)], the imaginary part grows only logarithmically. Resonances satisfying Siegert boundary conditions are square integrable and lie in the complex plane at an angle $-\beta$, where $\tan\beta=|E_I/E_R|$ in the section between $-\theta$ and the energy axis provided that $(2\theta-\beta)>0$ [13,14] (see Fig. 1). Here and in the following we set $v_0=10^{-4}$, $R=100$.

IV. NUMERICAL RESULTS

The efficiency of the various methods of suppressing reflections is quantitatively analyzed in this section employing a simple, analytically solvable model, namely, the propagation of a free radial wave packet. In order to satisfy the boundary condition at $r=0$ for all t, we choose at $t=0$ the antisymmetric linear combination of Gaussian wave packets

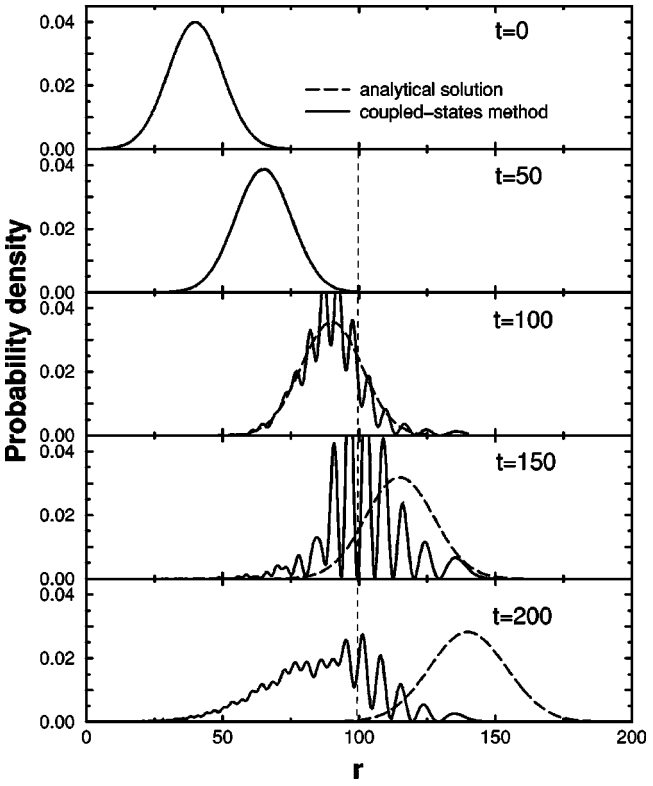

FIG. 2. Comparison of the analytical wave packet (dashed lines) and the unitary coupled-state results obtained using Sturmian pseudostates with $N=70$ and $n_S=1$ (solid lines). The initial Gaussian wave packet has a peak at $r_0=40$ with a width $\sigma=10$ and an average momentum $k_0=0.5$. The vertical dashed line is the approximate position of the reflecting wall.

$$\psi(r,0)=A\left\{\exp\left[-\frac{(r-r_0)^2}{4\sigma^2}+ik_0r\right]-\exp\left[-\frac{(r+r_0)^2}{4\sigma^2}-ik_0r\right]\right\}, \tag{55}$$

where A is a normalization constant, k_0 is the initial (mean) momentum of the wave packet, r_0 its mean position, and σ its radial width. If $(r_0+k_0t)^2\gg\sigma^2+t^2/4\sigma^2$, the analytic solution of the free-particle time evolution is given by

$$|\psi(r,t)|^2\simeq\frac{2(A\sigma)^2}{\sqrt{t^2+4\sigma^4}}\exp\left[-\frac{2\sigma^2\{r-(r_0+tk_0)\}^2}{t^2+4\sigma^4}\right] \tag{56}$$

and will be used in the following as a benchmark of the methods outlined above to represent reflection-free propagation where the wave packet is about to leave the inner region.

Figure 2 illustrates the reflection at the boundary of the coupled-state radial wave packet calculated using Sturmian pseudostates [Eq. (20)]. According to Eq. (7), the soft wall is localized around $r\approx1.5n_SN\approx100$ (for $n_S=1$, $N=70$) which is in good agreement with the onset of reflection in Fig. 2. As

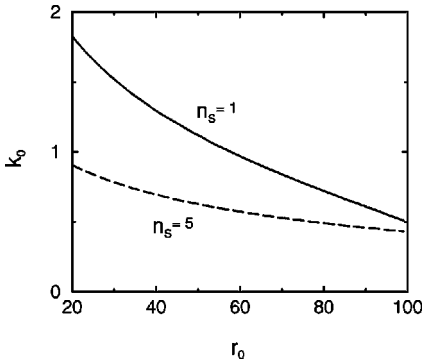

FIG. 3. Lines of constant Δ, i.e., $\mathcal{L}^2$ deviation of the approximate from the exact wave function, for two different Sturmian parameters ($n_S=1$ or 5). Above (below) each curve Δ is bigger (smaller) than 0.1. $N=70$ is used as a basis size.

the wave packet approaches the wall to within the approximate width, oscillations due to interference with the reflected portion become visible. At larger evolution times, the exact solution and the Sturmian pseudostate expansion have completely diverged from each other. While the wave packet has moved out to large distances and has completely left the inner region, the pseudostate expansion describes a unitary transformation within the inner region subtended by the truncated expansion and retains the whole wave packet.

It is instructive to analyze the k_0 dependence of the reflection. Whether or not a reflection occurs is directly associated with whether or not the wave packet can be localized in the basis set. Therefore, as a figure of merit we introduce the $\mathcal{L}^2$ distance between the exact ψ and projected $\psi_{\rm proj}$ wave packet,

$$\Delta=\int_0^\infty dr|\psi(r)-\psi_{\rm proj}(r)|^2, \tag{57}$$

$$|\psi_{\rm proj}\rangle=\sum_{n=0}^{N}\langle\phi_n^S|\psi\rangle|\phi_n^S\rangle. \tag{58}$$

Figure 3 displays lines of constant Δ for different values of the Sturmian parameter n_S and a fixed width of the wave packet $\sigma=10$ in the (k_0,r_0) plane. The contours are given for the value $\Delta=0.1$ such that the wave packet is well localized in the basis set. As can be anticipated from Eqs. (7) and (11), the contour lines form (approximate) hyperbolas with $k_0r_0\approx$const. Moreover, with decreasing n_S, the range of k_0 for a given r_0 supported by the basis set increases. Note, however, that $n_S\to0$ is not a viable strategy to avoid reflection since for small n_S the error Δ for representing well-localized atomic initial states will eventually increase.

The dependence of the effective position of the reflecting wall on the momentum can be analyzed in terms of the local density of the states $\mathcal{D}_{\rm loc}$,

$$\mathcal{D}_{\rm loc}(r,E)=\sum_n|\psi_n(r)|^2\delta(E-E_n), \tag{59}$$

where ψ_n are the eigenstates of the free-particle Hamiltonian [Eq. (3)] diagonalized in the truncated Sturmian basis. Figure 4 displays the LDOS (averaged over $\Delta r=16$) as a function

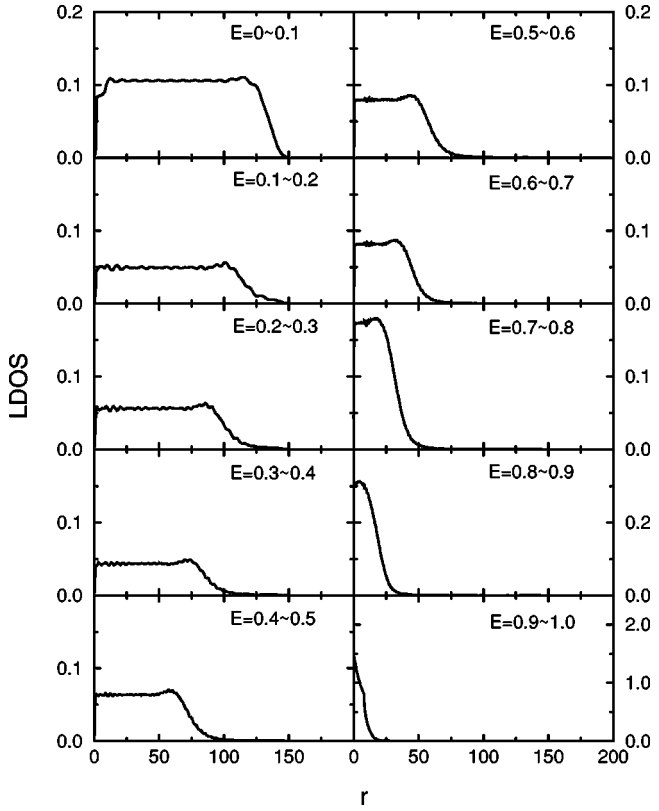

FIG. 4. Local density of states using a Sturmian basis with ($n_S=1$, $N=70$). Each graph is averaged over E ($\Delta E=0.1$) and r ($\Delta r=16$).

of r for different energy bins. Low-energy (low-k) states have a near-uniform high density out to large r. With increasing energy (momentum), decreasing ranges of r can be supported. This property of the LDOS provides the underpinning of the relation [Eq. (11)]. The consequence of this observation is that a Sturmian basis provides an adequate representation of the near-threshold continuum but may fail for the emission of energetic electrons. Equation (11) is a useful simple tool for estimating the dynamical range of the representation of the continuum by a Sturmian basis.

We turn now to alternative techniques for suppression of reflections. For reference, we show in Fig. 5 the standard masking technique for a lattice-based expansion where we use here the DVR expansion. As a masking function in Eq. (22) we used $f(r)=\sin^4[\pi(r-r_M)/2(r_N-r_M)]$ if $r>R$, $r_N=R=90$, and $r_M=100$. Note that we present a result from the masking method as a reference but using a masking function which is not necessarily the best for this problem. The momentum of the wave packet is $k_0=0.5$ and the time step for application of the nonunitary operator [Eq. (23)] is $\Delta t=50$ a.u. As the wave packet reaches the masking region, it gets distorted and altered. There is, however, a small but finite fraction of the wave packet that is reflected. For a given width and momentum of the wave packet, one can fine tune the masking function to reduce the distortion and the reflection. However, both features cannot be eliminated completely. In realistic wave packet propagations describing ionization, the broad distribution in both energy and position of a coherent excitation makes the optimization of fine tuning difficult.

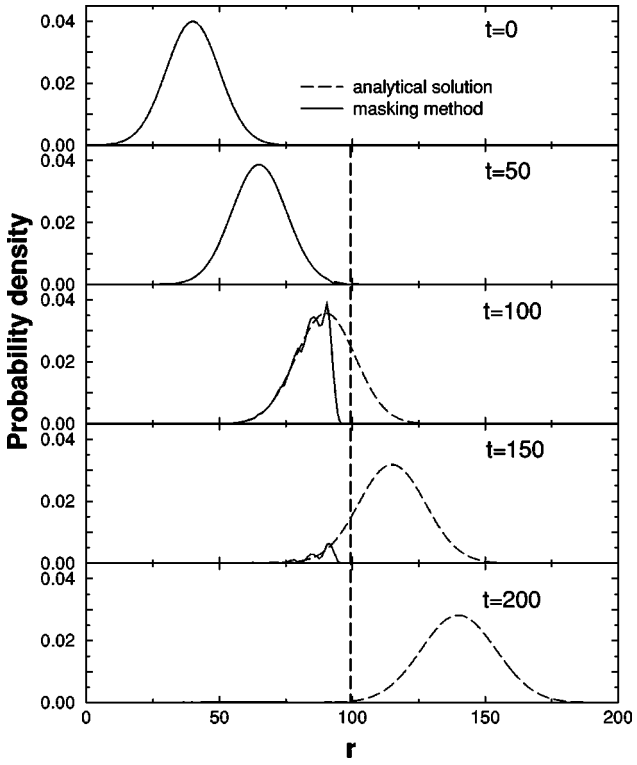

FIG. 5. Comparison of the analytical wave packet (dashed lines) and the results obtained using DVR basis states and a masking function (solid line) (see text). The initial wave packet is the same as that in Fig. 2.

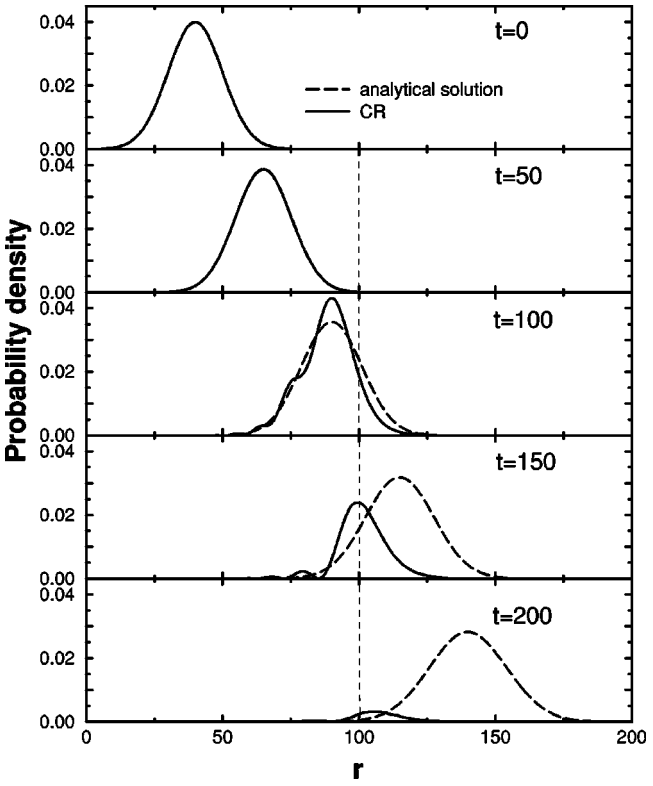

FIG. 6. Comparison of the analytical wave packet (dashed lines) and the complex rotation results using a Sturmian basis with $n_S=1$, $N=70$, and an angle $\theta=0.05$ (solid lines). The initial wave packet is the same as that in Fig. 2.

Figure 6 illustrates that evolution of the same wave packet in a complex-rotated basis also provides for a nonunitary evolution and an approximate suppression of reflection. The origin of the loss of probability is damping due to the complex energy spectrum [Eq. (43)]. An optimization at a high level of transmission through the wall (i.e., absorption) without significant distortion in the inner region could be accomplished by tuning to a small rotation angle of $\theta=0.05$ rad $=2.86°$. For such small rotation angles, the effective region of phase space that can be represented by the rotated basis is very similar to that of the unrotated basis.

The RPM provides an alternative tool to realize masking in an atomic pseudostate expansion without losing the advantage of using atomiclike states which may be helpful for describing the bound-state portion of the spectrum. Figure 7 presents an example for the same wave packet as in Figs. 2, 5, and 6 but now with repetitive projection applied with $N=70$, and $M=120$. Clearly, the projection-induced masking introduces some distortion of the wave packet similar to the one observed for complex rotation or lattice-based masking method. The distortion is, however, confined to the masking region. Only when $r_0\approx 100$ and is close to the ''wall,'' do distortions due to interferences become visible while the inner region remains unaffected.

It is now of interest to explore the efficiency and tunability of the RPM. Figure 8 shows the transmission probability through the wall (i.e., the loss of probability from the ''inner'' region) as a function of the time interval Δt between successive projections and different k_0. For different values of k_0, the transmission probability reaches $\gtrsim 90\%$ for the same range of $\Delta t\approx 5-50$. Consequently, for a wide range of k values (variation by a factor 4) and energies (factor 16), a large amount of suppression of reflections can be achieved.

The transmission curves show a rapid falloff from the maximum towards larger Δt as well as smaller Δt. The reduced transmission through the wall, or equivalently, enhanced reflection for large Δt has a simple ''geometric'' interpretation. If the time interval exceeds the round-trip time through the ''masking region'' of length ΔR,

$$\Delta t \geqslant 2\Delta R/k_0, \tag{60}$$

the wave packet is reflected at the ''outer wall'' associated with the border of the domain $P+Q'$ to the inner region (states ϕ_n with $n\leqslant N$) before the next projection takes place. Note that the discontinuous dropoff in Fig. 8 for $k_0=1$ occurs when Δt changes abruptly from $\Delta t=t$ to $\Delta t=t/2$ corresponding to $J=1,2$ (the total propagation time for the smaller momenta is, in turn, outside of the time range in the figure).

More interestingly, the transmission is also reduced when the projection is performed too often, i.e., when Δt is too small. This is nothing but the manifestation of the onset of the quantum Zeno effect [26], here observed for the free-particle wave packet evolution. Its physical interpretation is that by projecting too often, the evolution of the wave packet is ''frozen'' inside the P space which prevents the transmission and the leakage out. For the limit $\Delta t\to 0$ this can be easily shown as follows: Using the decomposition [Eq. (24)] we find for small Δt

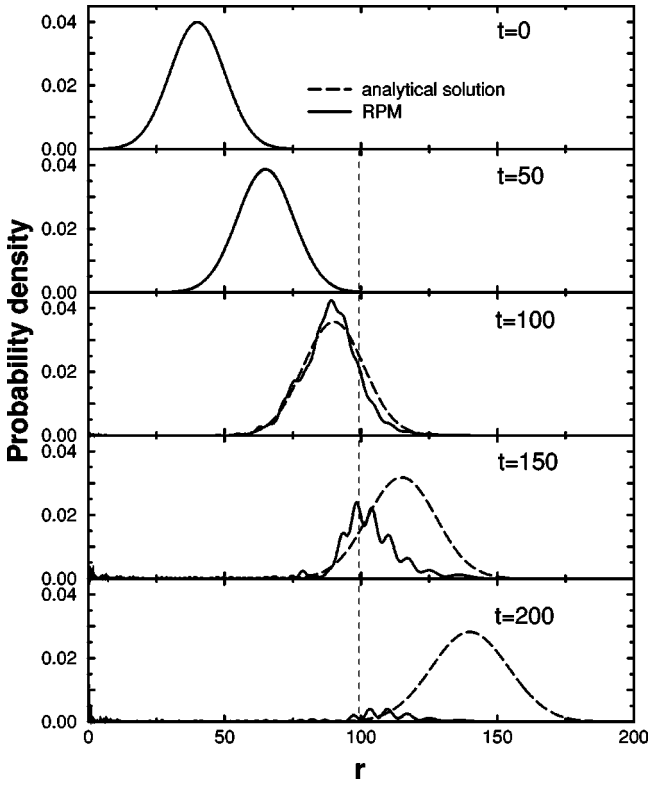

FIG. 7. Comparison of the analytical wave packet (dashed lines) and the results of the repetitive projection method (RPM) using Sturmian pseudostates with $N=70$, $M=120$, and $n_S=1$ (solid lines). The initial wave packet is the same as that in Fig. 2.

$$|P+Q'\rangle e^{-i\langle P+Q'|H|P+Q'\rangle\Delta t}\langle P+Q'|P\rangle \simeq |P\rangle(1-i\langle P|H|P\rangle\Delta t)+|Q'\rangle(-i\langle Q'|H|P\rangle\Delta t). \tag{61}$$

Therefore,

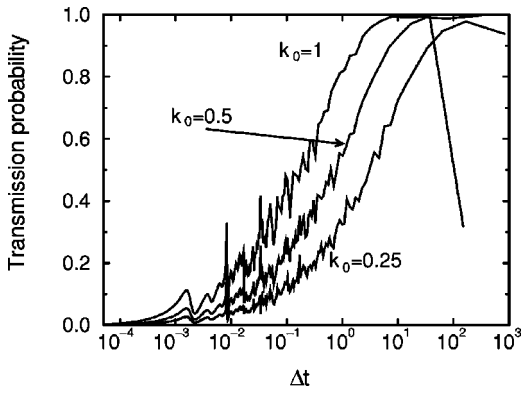

FIG. 8. Transmission probability through the wall generated by the repetitive projection method. Each curve corresponds to a different momentum and total propagation time t such that 99% of the exact wave packet should go through the inner wall. For $k_0=0.25$ $t=830$, for $k_0=0.5$ $t=320$, and for $k_0=1$ $t=150$. The parameters for the initial wave packet are $\sigma=10$ and $r_0=30$. The parameters for the basis sets used in this calculation are $N=70$, $M=120$, and $n_S=1$.

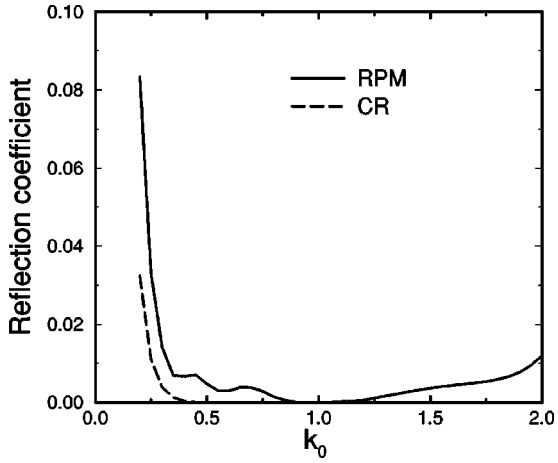

FIG. 9. Reflection coefficient as a function of mean momentum value k_0 of the initial wave packet with $r_0=40$ and $\sigma=10$. The RPM (solid line) calculation was performed using $n_S=1$, $N=70$, $M=270$, and $\Delta t=80$. For the complex rotation method (CR: dashed line) we used $N=70$, $n_S=1$, and $\theta=0.05$.

$$\langle P|P+Q'\rangle e^{-i\langle P+Q'|H|P+Q'\rangle\Delta t}\langle P+Q'|P\rangle \simeq 1-i\langle P|H|P\rangle\Delta t-\frac{1}{2}\langle P|H|P\rangle^2\Delta t^2-\frac{1}{2}\langle P|H|Q'\rangle \times\langle Q'|H|P\rangle\Delta t^2. \tag{62}$$

Note that there are no couplings to the Q' space to first order in Δt but only to second order $\sim\Delta t^2$. If we take a fixed evolution time t and J time steps, $\Delta t=t/J$, we find in the limit $J\to\infty$

$$\begin{aligned}\langle P|P+Q'\rangle e^{-i\langle P+Q'|H|P+Q'\rangle J\Delta t}\langle P+Q'|P\rangle &\simeq[\langle P|P+Q'\rangle e^{-i\langle P+Q'|H|P+Q'\rangle\Delta t}\langle P+Q'|P\rangle]^J \\ &\simeq(1-i\langle P|H|P\rangle\Delta t)^J-\frac{J\Delta t^2}{2}\langle P|H|Q'\rangle\langle Q'|H|P\rangle \\ &\simeq 1-i\langle P|H|P\rangle t-\frac{t}{2}\langle P|H|Q'\rangle\langle Q'|H|P\rangle\Delta t.\end{aligned} \tag{63}$$

Therefore, in the limit $J\to\infty$, $\Delta t\to 0$, and $J\Delta t=t$ $=$const, the coupling to the Q' space vanishes. This is the direct analog to the quantum Zeno effect in spin systems. In the present case, it corresponds to the complete eradication of the masking effect and the replacement by a complete reflection at the boundary between the interaction region and the masking region. This—at first counterintuitive—result is the essence of the quantum Zeno effect. The decrease of transmission in Fig. 8 with decreasing Δt can therefore be considered as the onset of this effect which is completely realized at $\Delta t\lesssim 10^{-4}$.

In Fig. 9, a typical dependence of the reflection coefficient as a function of the momentum of the wave packet, k_0 is displayed for both the CR and the RPM methods. The reflection coefficient in this case is defined as the probability to find the electron in the interval $[0,100]$ after a long enough time such that the whole wave packet is outside this interval. Note that the calculations in the figure have been obtained

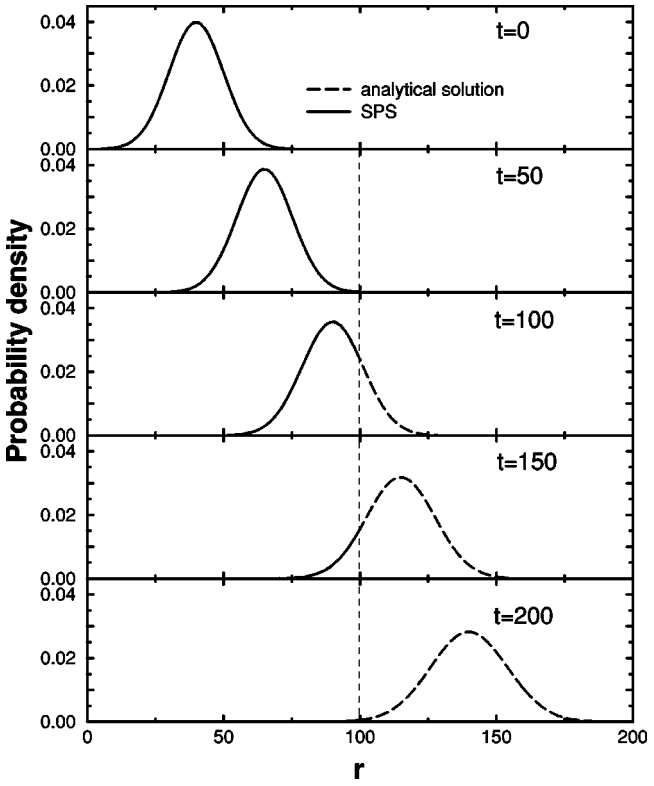

FIG. 10. Comparison of the analytical wave packet (dashed lines) and the results obtained using $N=50$ Siegert pseudostates generated by 100 DVR basis functions (solid lines). The initial wave packet is the same as that in Fig. 2.

using a fixed basis set and a fixed value of Δt, i.e., we intentionally avoid any optimization of the reflection coefficient as a function of k_0. For this particular set of parameters, reflections can be reduced to less than 1% for $0.3 \leqslant k_0 \leqslant 2$, which corresponds to an energy variation by more than a factor 40. Clearly, this ''applicability range'' can be increased and shifted by appropriately tuning Δt, n_s, N, and M. For this free-particle time evolution problem, CR can suppress the reflection more effectively. However, in problems with nondilatation analytic potential [i.e., the case E^I in Eq. (43) becomes positive] an implementation of CR is less obvious. For such cases, the RPM can be considered as a viable alternative within the framework of atomic pseudostate expansions.

Finally, the SPS basis provides a very efficient method for suppressing reflections. Figure 10 displays the propagation of the wave packet with the same parameters ($k_0=0.5$, $\sigma=10$) as in the previous example. Obviously, the SPS propagation allows for virtually perfect transmission through the boundary. Moreover, in contrast to the lattice-based masking function (Fig. 5), the complex rotation (Fig. 6), and the RPM (Fig. 7), the wave packet remains virtually undisturbed near the boundary. The SPS basis shares many common features with the complex scaling calculation (Fig. 6), in particular the complex energy propagation. It is therefore interesting to further inquire into the differences for the wave packet propagation employing the two methods. The key is the difference in the spectral distributions of the energies in the complex plane (Fig. 1). While within the complex scaling approach the energies lie on a ray of fixed angle θ with

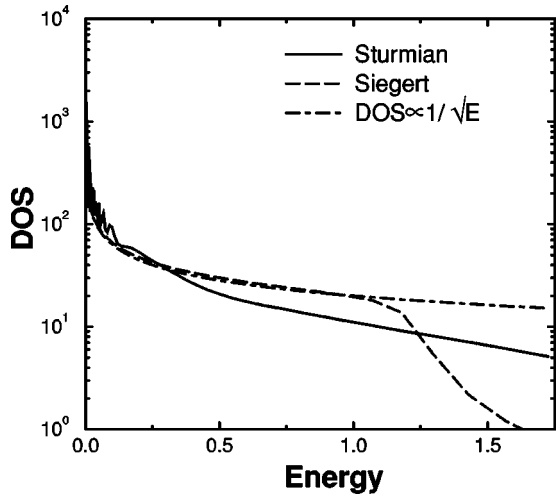

FIG. 11. Comparison of the spectral densities obtained using $N=70$ complex Sturmian states with $n_S=70$ and $\theta=0.05$ (dashed line) and $N=50$ Siegert states constructed from 100 DVR states and with $R=100$ (solid line).

respect to the real energy axis and both real and imaginary parts of E grow at the same rate, the imaginary part of the energies of the SPS is weakly dependent on the real part and is almost constant for large k values. For the time propagation up to $t \lesssim 100$ the relevant region of the spectrum should be such that $E_n^I t \lesssim 1$, or $E_n^I \lesssim 10^{-2}$ (such that the probability is not yet absorbed). In this region, both spectral densities are quite similar. One may therefore interpret the efficiency of the complex rotation method in terms of the proximity of the complex rotation spectrum to the one of the most relevant Siegert states.

The range of energies and momentum of wave packets which can be represented in a given SPS basis depends, of course, not only on the amount of suppression of reflection but also on the effective spectral density of states $\mathcal{D}$ in the region of physical interest,

$$\mathcal{D}(E) = -\frac{1}{\pi} \sum_n \mathrm{Im}\left(\frac{1}{E-E_n}\right), \tag{64}$$

where E_n represents a complex eigenvalue [in the limit $\mathrm{Im}(E_n) \to 0$ one obtains a sum of δ functions as in Eq. (59)]. Figure 11 gives a comparison of the spectral density of the same number of positive-energy states using the complex Sturmian pseudostates and the SPS. For reference, we show also the DOS for a free particle in a one-dimensional box, $\mathcal{D} \propto 1/\sqrt{(E)}$. Obviously, the spectral weight is differently distributed in the two methods. The Sturmian pseudostates place an increased spectral weight in the near-threshold region relative to the free-particle DOS while underrepresenting high-energy continuum states. This is a direct consequence of the effective momentum dependence of the position of the wall [Eq. (11)]. The SPS states, on the other hand, follow closely the free-particle behavior of the DOS. These differences may also influence the choice of the optimal basis set depending on the process to be investigated. For near-threshold processes, the Sturmian pseudostates may be advantageous while for high-energy electron emission the SPS may be more appropriate.

V. CONCLUSION

We have performed a comparative study of different methods of wave packet propagation described by a time-dependent Schrödinger equation within atomic pseudostate expansions. We have proposed two techniques which are designed to control unphysical reflections. One is the extension of the notion of masking functions, well known for grid-based expansions [7–10], to equivalent projection operators for atomic pseudostates, as specifically implemented for Sturmian basis states. The other one is the application of Siegert pseudostates, well known for time-independent scattering theory for resonances [23,24], to the study of wave packet evolution. Both methods provide efficient techniques for suppressing reflections. The SPS method features the added benefit that the suppression of reflections does not cause significant distortions of the wave packet near the boundary where reflections take place. The present test for the free-particle evolution may serve as a benchmark for complex problems such as the periodically kicked Rydberg atom which features complex, nonseparable dynamics and where no exact analytical solution is available.

ACKNOWLEDGMENTS

This work was supported by the NSF and by U.S. DOE Office of Basic Energy Sciences, Division of Chemical Sciences under Contract No. DE-AC05-96OR22646 with Lockheed Martin Energy Research Corporation. S.W. acknowledges with gratitude the support by Monbusho (Ministry of Education, Science, Sports, and Culture of Japan).

[1] M. V. Berry, Physica D **33**, 26 (1988); J. M. Robbins and M. V. Berry, J. Phys. A **25**, L961 (1992).
[2] See, e.g., H. Schuster, *Deterministic Chaos* (VCH Publishers, Weinheim, 1988).
[3] E. Ott, *Chaos in Dynamical Systems* (Cambridge University Press, New York, 1993).
[4] A. K. Dhar, M. A. Nagaranjan, F. M. Izrailev, and R. R. Whitehead, J. Phys. B **16**, L17 (1983); A. Carnegie, *ibid.* **17**, 3435 (1984); T. P. Grozdanov and H. S. Taylor, *ibid.* **20**, 3683 (1987); J. Burgdörfer, Nucl. Instrum. Methods Phys. Res. B **42**, 500 (1989).
[5] C. F. Hillermeier, R. Blümel, and U. Smilansky, Phys. Rev. A **45**, 3486 (1992); M. Melles, C. O. Reinhold, and J. Burgdörfer, Nucl. Instrum. Methods Phys. Res. B **79**, 109 (1993).
[6] G. Casati, I. Guarneri, and G. Mantica, Phys. Rev. A **50**, 5018 (1994); H. Wiedemann, J. Mostowski, and F. Haake, *ibid.* **49**, 1171 (1994).
[7] R. Heather and H. Metiu, J. Chem. Phys. **86**, 5009 (1987).
[8] P. Schwendner, C. Beck, and R. Schinke, Phys. Rev. A **58**, 2203 (1998).
[9] J. C. Wells, D. R. Schultz, P. Gavras, and M. S. Pindzola, Phys. Rev. A **54**, 593 (1996); D. R. Schultz *et al.*, *ibid.* **50**, 1348 (1994).
[10] J. L. Krause, K. J. Schafer, and K. C. Kulander, Phys. Rev. A **45**, 4998 (1992).
[11] See, e.g., D. Neuhauser and M. Baer, J. Chem. Phys. **90**, 4351 (1989).
[12] S. D. Parker and C. W. McCurdy, Chem. Phys. Lett. **156**, 483 (1989).
[13] W. P. Reinhardt, Annu. Rev. Chem. **33**, 223 (1982).
[14] Y. K. Ho, Phys. Rep. **99**, 1 (1983).
[15] A. Maquet, S. I. Chu, and W. P. Reinhardt, Phys. Rev. A **27**, 2946 (1983).
[16] M. Pont, D. Proulx, and R. Shakeshaft, Phys. Rev. A **44**, 4486 (1991).
[17] J. F. Reading and A. L. Ford, J. Phys. B **12**, 1367 (1979).
[18] X. Wang and D. Dill, J. Phys. B **31**, L891 (1998).
[19] J. C. Light, I. P. Hamilton, and J. V. Lill, J. Chem. Phys. **82**, 1400 (1985), and references therein. The DVR method in the present article is based on Jacobi polynomials as described in Ref. [25].
[20] M. Rotenberg, Adv. At. Mol. Phys. **6**, 233 (1970).
[21] S. Yoshida, C. O. Reinhold, J. Burgdörfer, B. E. Tannian, R. A. Poppole, and F. B. Dunning, Phys. Rev. A **58**, 2229 (1998).
[22] H. Bethe and F. Salpeter, *Quantum Mechanics of One- and Two-Electron Atoms* (Plenum, New York, 1977).
[23] B. Schneider, Phys. Rev. A **24**, 1 (1981).
[24] O. I. Tolstikhin, V. N. Ostrovsky, and H. Nakamura, Phys. Rev. Lett. **79**, 2026 (1997).
[25] O. I. Tolstikhin, V. N. Ostrovsky, and H. Nakamura, Phys. Rev. A **58**, 2077 (1998).
[26] B. Misra and E. C. G. Sudarshan, J. Math. Phys. **18**, 756 (1977); A. Peres, Am. J. Phys. **48**, 931 (1980).